THE JOURNAL OF PHYSICAL CHEMISTRY C

Article

Cite This: J. Phys. Chem. C 2019, 123, 10051−10056

pubs.acs.org/JPCC

Stability of Zirconium Carbide under High Pressure and High Temperature

Lijie Tan,[†,‡] Zhidan Zeng,[*,‡] Hongbo Lou,[‡] Fei Zhang,[‡] Xiehang Chen,[‡] Songyi Chen,[‡] Yuanyuan Xuan,[‡] Fang Peng,[*,†] and Qiaoshi Zeng[‡,§]

[†]Institute of Atomic and Molecular Physics, Sichuan University, Chengdu 610065, People's Republic of China

[‡]Center for High Pressure Science and Technology Advanced Research (HPSTAR), Pudong, Shanghai 201203, People's Republic of China

[§]Jiangsu Key Laboratory of Advanced Metallic Materials, School of Materials Science and Engineering, Southeast University, Nanjing 211189, People's Republic of China

S *Supporting Information*

ABSTRACT: As a prototype refractory and hard transition-metal carbide, the stability of zirconium carbide (ZrC) under extreme conditions is critical for its applications. Despite the extensive theoretical studies, few experimental results are available until now. In this work, we carried out a comprehensive experimental study of ZrC in a large unexplored pressure−temperature region (up to ∼150 GPa and ∼2000 K) by combining in situ high-pressure and high-temperature synchrotron radiation X-ray diffraction with various ex situ characterization techniques. Our results demonstrate that ZrC (B1 phase) remains stable up to ∼154 GPa at room temperature or at ∼40 GPa up to 2000 K, rather than undergoing the predicted B1-to-B2 phase transition. However, under high pressure and temperature, ZrC is extremely active when water is present. It would react with even trace amount of absorbed water to form ZrO_2 and CH_4. Our results clarify the structural and chemical stability of ZrC at extreme conditions, which would guide the applications of ZrC and provide new experimental constraint for theoretical calculations.

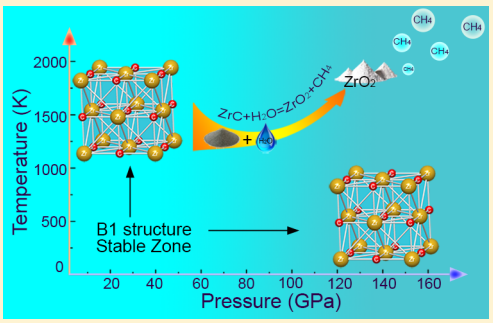

Downloaded by FUDAN UNIV at 02:09:43:294 on July 03, 2019
from https://pubs.acs.org/doi/10.1021/acs.jpcc.9b00715.

I. INTRODUCTION

The carbides of transition metals are well known as refractory materials and exhibit desirable physical and chemical properties associated with their unique bonding character constituting covalent, metallic, and ionic nature. These transition-metal carbides (TMCs) are unique materials that could combine the characteristic properties of ceramics and metals. For instance, they possess extreme hardness and very high melting temperatures, which are typical properties of covalent materials; they also show luster, high electrical and thermal conductivities like metals, and have NaCl-type structure (B1), a typical structure of ionic materials.[1−6] Due to the mixed bonding between metal and carbon atoms, TMCs are also excellent catalysts capable of challenging noble metals.[2] Recently, these metallically conductive and even superconducting TMCs emerge as interesting new two-dimensional materials and have attracted broad research interest.[7−9]

Zirconium carbide (ZrC) as one of the prototype transition-metal carbides has been intensively studied.[10−13] ZrC owns many extraordinary properties such as very high melting temperature (3530 °C),[14] excellent thermal stability in oxygen-free environments, exceptional mechanical hardness (∼30 GPa), strength and wear resistance,[15] chemical inertness, and imperviousness to hydrogen attack.[16] Meanwhile, it possesses excellent ionic and electronic conductivity. These properties make ZrC promising in widespread industrial applications, especially in extreme high-pressure and high-temperature (HPHT) environments.[17,18]

The structural stability of ZrC at extreme conditions is, of course, one of the most important topics. High pressure is not only a unique approach for novel material synthesis, especially hard or superhard materials such as nanotwined diamond, amorphous diamond, and nanotwined cubic-BN, VB_2, CrB, and Ir_2P[19−24] but also an important parameter to investigate the structural stability of the materials. A phase transformation from NaCl-type (B1 phase) to CsCl-type (B2 phase) structure under high pressure has been predicted by theoretical calculations.[25−31] However, the transition pressures predicted by various theoretical calculations are not consistent, ranging from ∼98 to ∼300 GPa.[25−31] So far, there is no experimental study on the stability and phase transitions of ZrC at ultrahigh pressure and temperature.

In this work, we utilize in situ high-pressure and high-temperature synchrotron radiation X-ray diffraction (XRD) and a bunch of ex situ characterization techniques to study the structural evolution of ZrC in an unexplored HPHT region.

Received: January 25, 2019
Revised: February 26, 2019
Published: March 28, 2019

© 2019 American Chemical Society

DOI: 10.1021/acs.jpcc.9b00715
J. Phys. Chem. C 2019, 123, 10051−10056

The stability of ZrC up to 154 GPa and 2000 K has been experimentally clarified.

II. EXPERIMENTS

II.I. Sample Loading for High-Pressure Experiments. In situ high-pressure synchrotron radiation XRD experiments at ambient temperature were performed in a symmetric diamond anvil cell (DAC) with a culet size of 300 μm. The sample chamber was a 120 μm diameter hole drilled in the center of the indent of a preindented T301 stainless steel gasket. ZrC powder (purity 99.99%, from Aladdin Co., Ltd.) was pressed to a disk with a thickness ~25 μm and loaded into the sample chamber. Two tiny ruby balls were loaded along with the sample. The ruby fluorescence peak shift was used for pressure calibration.[32] Helium was used as the pressure medium to provide ideal hydrostatic conditions. The ZrC sample was compressed up to ~43 GPa. A symmetric DAC with a beveled anvil culet of 300−150 μm (bevel angle of 10°) was used for another experiment up to ~150 GPa. Rhenium was used as the gasket material. The gold powder was loaded into a 40 μm diameter sample chamber as the pressure standard material along with the ZrC sample without a pressure medium.[33]

For HPHT experiments, symmetric DACs with 300 μm culets were used. The ZrC powder was sandwiched by sodium chloride (NaCl) or magnesium oxide (MgO), which acted as a pressure medium, a pressure calibrant, and a thermal insulator. The NaCl/MgO powders were baked for hours at 120 °C before loading into the DAC. To remove any possible moisture absorbed in NaCl/MgO during the sample loading, the sample was baked again at 120 °C for half an hour after sample loading before sealing the DAC.

II.II. In Situ High-Pressure (High-Temperature) Synchrotron Radiation XRD Experiments. In situ high-pressure synchrotron radiation XRD experiments were performed at the beamline 12.2.2 (X-ray wavelength λ = 0.4959 Å, beam size = 10 × 10 μm^2) at the Advanced Light Source (ALS), Lawrence Berkeley National Laboratory (LBNL) and at the beamline 13 ID-D (λ = 0.3220 Å, beam size = 3 × 4 μm^2) at the Advanced Photon Source (APS), Argonne National Laboratory (ANL).[34,35] A MAR345 image plate and a MAR165 charge-coupled device detector were used for data collection, respectively. The software Dioptas was used to integrate the two-dimensional diffraction images into XRD patterns.[36] For HPHT experiments, a double-side YLF (wavelength 1064 nm) laser-heating system was used to heat the sample. Temperatures were determined by fitting the thermal radiation spectra of the heated sample to the Planck radiation function in a given wavelength range.

II.III. Other Techniques. The Raman spectra of the HPHT-treated ZrC samples were measured at ambient conditions using a micro-Raman spectroscopy system (Renishaw, in Via Reflex) with a 532 nm laser beam as the excitation source. The laser spot size was approximately 2 μm. The scanning electron microscopy (SEM) and energy-dispersive X-ray spectrometry (EDS) experiments were carried out on the HPHT-treated ZrC samples using a field emission SEM (FEI VERSA 3D dual beam). The thermogravimetric (TG) analysis testing was performed on the initial ZrC powders using a NETZSCH TG 209 F3 Tarsus system.

III. Results and Discussion. Figure 1a shows the XRD patterns of the ZrC sample as a function of pressure up to ~43 GPa. All the peaks shift to higher 2θ angels during compression. No new peak emerges. The XRD peak positions (2θ) were derived by fitting each peak using a Voigt line profile after subtracting the baseline. The d-spacing corresponding to each peak was calculated according to the Bragg equation ($d = \lambda/2 \sin\theta$). As shown in Figure 1b, the d-spacings decrease smoothly with increasing pressure. These results indicate that the B1 structure of ZrC remains stable up to 43 GPa at room temperature. In addition, the lattice parameters and unit-cell volumes of ZrC under pressure were obtained through refinement. The unit-cell volume decreases by ~15% from 0 to 43 GPa (see Figure 1c). The unit-cell volume as a function of pressure can be well fitted to the third-order Birch−Murnaghan equation of state,[37] which yields the isothermal

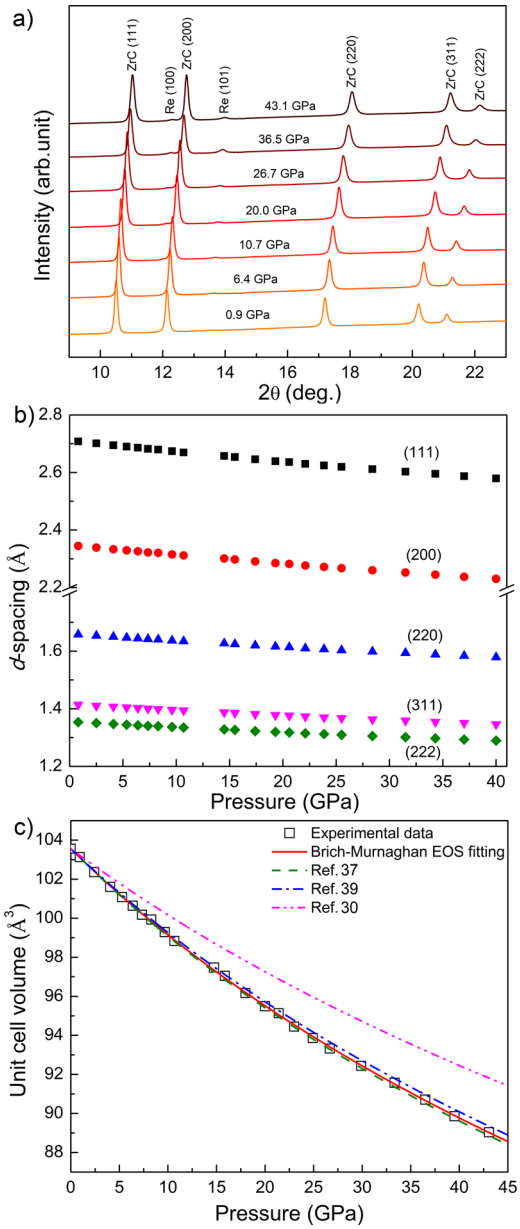

Figure 1. In situ high-pressure XRD study of ZrC with helium as the pressure medium at room temperature. (a) The XRD patterns at different pressures up to ~43 GPa. (b) The diffraction peak position as a function of pressure. (c) The unit-cell volume as a function of pressure and comparison with literature data (ref 38: ultrasonic measurement, refs 40 and 31: density functional theory (DFT) simulations). The X-ray wavelength is 0.4959 Å.

DOI: 10.1021/acs.jpcc.9b00715
J. Phys. Chem. C 2019, 123, 10051−10056

bulk modulus at ambient pressure K_0 = 210(1) GPa and its derivative K_0' = 4.0(1). With the best hydrostatic pressure condition provided by helium as the pressure medium, the K_0 and K_0' values are accurately derived with minimized experimental uncertainty. The bulk modulus obtained in our experiments is consistent with the adiabatic bulk modulus derived from previous ultrasonic measurements (K_{0s} = 207 GPa).[38] It is also close to the values reported by most theoretical calculations,[28−30,39] e.g., K_{0s} = 217 GPa derived from the Debye−Grauneisen model.[40] The bulk modulus yielded by the ab initio calculations based on pseudopotential approach (K_{0s} = 283 GPa) is relatively higher.[31]

Since theoretical calculations predict that B1-to-B2 phase transition of ZrC might happen at ultrahigh pressures above 98 GPa,[27] another experiment with a much higher pressure up to ∼154 GPa was further conducted. The in situ high-pressure XRD patterns are shown in Figure 2. With increasing pressure,

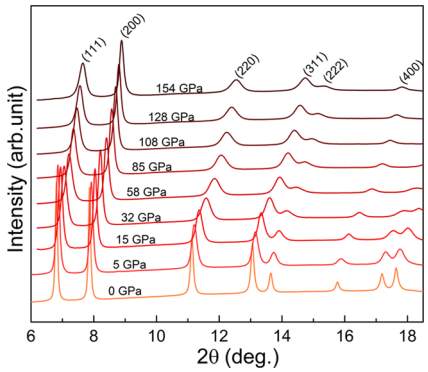

Figure 2. In situ ultrahigh-pressure study of ZrC without pressure medium at room temperature. The XRD patterns of ZrC at different pressures up to ∼154 GPa. The X-ray wavelength is 0.3220 Å.

all peaks shift to higher 2θ angles, without the emergence of any new peak. The peak width increases rapidly during compression, which could be attributed to the accumulated high deviatoric stress (pressure gradient) in the sample, since no pressure medium was used in this experiment.[41,42] This result confirms the high stability of B1 structure of the ZrC above 100 GPa even if strong deviatoric stress is present. Therefore, we conclude that the phase transition of ZrC from the NaCl-type phase to the CsCl-type phase predicted by many theoretical calculations does not occur during compression up to 154 GPa at room temperature.[27,29−31,43]

According to the theoretical calculations, the Gibbs free energy of the B2 phase should be lower than the B1 phase under high pressure. The experimental observation of the B1-to-B2 phase transition may be hindered by the significant energy barrier between the two phases, which would be rather difficult to overcome at room temperature. Therefore, combing high pressure with high temperature is necessary to clarify this possibility. With the double-side laser-heating technique, the ZrC sample was first compressed to different target pressures and then ramped up to ∼2000 K. Figure 3a shows the XRD patterns of one experiment with the constant pressure at 40 GPa and the temperature up to 1700 K. The XRD pattern before heating shows peaks from both the B1 phase ZrC and MgO (thermal insulator material). However, several new peaks marked by asterisk symbols appear after heating at the expense of the initial B1 phase ZrC, indicating the emergence of a new phase. Surprisingly, the intensity of these new diffraction peaks

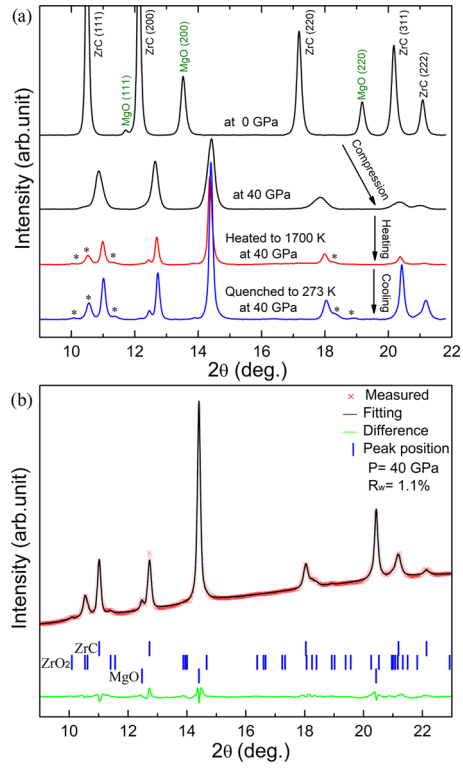

Figure 3. In situ high-pressure and high-temperature XRD measurement of ZrC. (a) Representative in situ XRD patterns of ZrC during compression to 40 GPa and at room temperature, heated to ∼1700 K, and quenched to room temperature. The X-ray wavelength is 0.4959 Å. Diffraction peaks from the ZrO_2 phase are marked by the asterisk. (b) The Rietveld refinement of the XRD pattern collected at 40 GPa and quenched from ∼1700 K after laser heating. MgO was used as pressure medium and thermal insulator. The initial B1 structure of ZrC and orthorhombic II (space group: *Pnma* (62)) structure of ZrO_2 are indexed.

almost did not change when the temperature was further increased to ∼2200 K. All the phases obtained after laser heating can be fully quenched to room temperature at 40 GPa. According to the Rietveld refinement of the XRD patterns of the quenched sample at 40 GPa (Figure 3b), the major phases are identified to be the initial B1 ZrC and MgO plus a small amount of orthorhombic high-pressure ZrO_2 (O-II, space group: *Pnma*).

Then, an interesting question is raised: Where does the oxygen come from in the sealed high-pressure chamber? Since the pressure medium MgO contains oxygen, intuitive speculation of the oxygen source is associated with MgO. To clarify this possibility, other experiments with NaCl or even high-purity neon gas as the pressure medium were performed. The same mixture of the initial B1 ZrC, NaCl, and orthorhombic II (O-II) ZrO_2 was obtained in a similar temperature and pressure range. In addition, we carried out four more experiments at different pressures (5, 10, 20, and 40 GPa) and temperatures from ∼1500 to ∼2000 K. Besides the initial B1 ZrC, the new peaks emerging at high temperatures can always be indexed into ZrO_2 with different crystal structures depending on the pressure and temperature conditions.[44] For example, the new X-ray reflections of the sample quenched from ∼2000 K at 5 GPa are confirmed to be the high-temperature and ambient-pressure phases of ZrO_2 with a tetragonal structure (space group: $P4_2/nmc$) (see

DOI: 10.1021/acs.jpcc.9b00715
J. Phys. Chem. C 2019, 123, 10051−10056

Supporting Information Figure S1). Furthermore, the formation of the O-II phase of ZrO_2 at HPHT was also confirmed by the Raman spectra (see Figure 4) according to previous

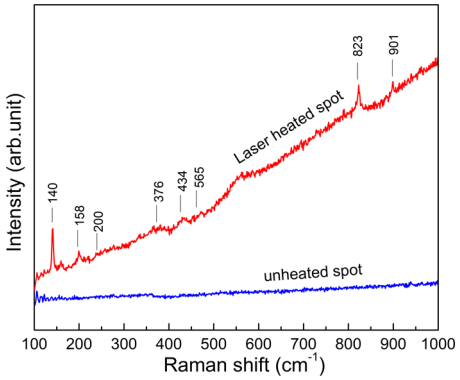

Figure 4. Raman spectra of the ZrC sample at ambient conditions quenched from 36 GPa and 2000 K: unheated area (blue) and laser-heated spot (red). Raman signal from the ZrO_2 (orthorhombic II) only presents in the laser-heated spot. In contrast, the unheated region shows no Raman signal. The excitation laser wavelength is 532 nm. The significant background signal shown in the red curve is caused by the typical strong fluorescence after laser heating.

research.[45] Only the laser-heated spots show the Raman peaks of ZrO_2; the other area remains intact. Also, the initial B1 ZrC sample shows no Raman peak as well. These results suggest that the initial ZrC sample contains no detectable ZrO_2; high temperature is necessary for the formation of ZrO_2 out of the ZrC sample. Hence, the oxygen should come from the sample itself rather than the pressure medium or the surrounding environment.

By using scanning electron microscopy (SEM) and energy-dispersive X-ray spectrometry (EDS), the chemical composition and its spatial distribution of the initial B1 phase ZrC sample were characterized. As shown in Figure S2a, the ZrC sample shows a typical morphology of polycrystalline powder with an average grain size of ~1 μm. According to the EDS result of the initial ZrC sample (Supporting Information Figure S2b), the compositions of different scanned regions are quite uniform. In addition to the predominant zirconium and carbon elements (with ratio close to ideal stoichiometry 1:1), ~6% (atomic percentage) oxygen element was surprisingly observed. Considering the vacuum environment of the EDS measurement, 6% is quite high. Therefore, it is not likely to be attributed to the absorbed oxygen molecules.

Another common oxygen source in our environment is H_2O. The initial ZrC may absorb H_2O moisture. Therefore, the initial sample (ZrC powder) were tested by TG to directly determine the content of H_2O. As shown in Figure 5, rapid mass loss was observed between ~74 and 100 °C, which agrees with the typical volatile temperatures of absorbed water. The mass loss continues up to ~375 °C, which suggests the strong interaction of ZrC and water and also may explain the difficulty of totally avoiding water in the ZrC sample in our experiments during baking. The total mass loss up to ~375 °C is ~1%, corresponding to a H_2O content of 5.5% (molar ratio), which is quite consistent to the result of EDS (~6%).

A DFT calculation together with atomistic thermodynamic modeling has been used to study the reactivity of the (111) and (110) facets of ZrC with H_2O, suggesting that the oxidized surface is much easier to functionalize than the bare ZrC(100)

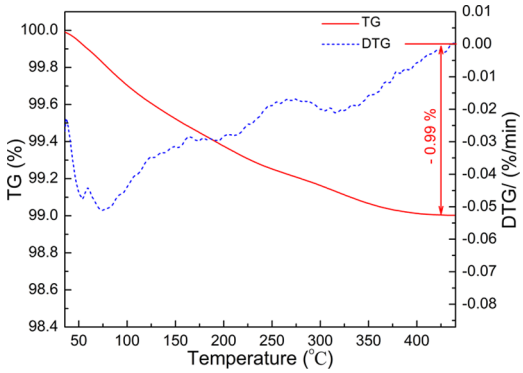

Figure 5. Characterization of the water content in the initial ZrC sample using differential thermal analysis/TG. The mass of the sample was ~20.083 mg. The heating rate was 10 K/min. The sample was put in an Al_2O_3 crucible and under high-purity N_2 atmosphere.

surface.[46,47] The corrosion of ZrC in water vapor above 650 °C at ambient pressure was recently found to produce ZrO_2, CO/CO_2, and H_2.[48] However, no theoretical or experimental studies on the reactivity of ZrC with water at both high pressure and high temperature have been reported. To confirm the reaction of ZrC with water and its products under high pressure and high temperature, we loaded the ZrC sample together with an excess amount of H_2O (as the pressure medium) in a DAC. Then, the ZrC sample was compressed to ~5 GPa at room temperature, followed by laser heating to approximately 2000 K. The entire sample quickly changed color from black to white after heating. The structure of the recovered samples was further studied by Raman spectroscopy. As shown in Figure 6, all characteristic active bands can be

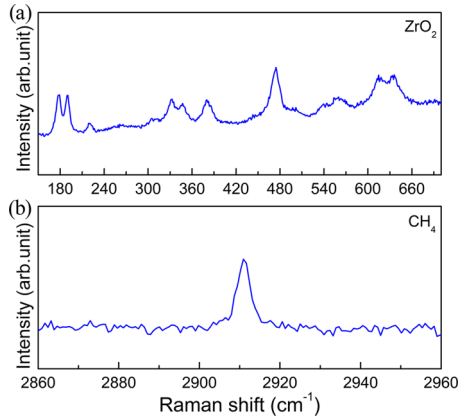

Figure 6. Raman spectra of the phases at ~0.8 GPa and room temperature obtained by reaction between the ZrC powder and pure water at ~5 GPa and ~2000 K. ZrO_2 and CH_4 can be identified by their characteristic Raman peaks. The excitation laser wavelength was 532 nm.

identified as those belonging to ZrO_2 (monoclinic, $P2_1/c$) and CH_4 (phase I, $Fm3m$).[49,50] Therefore, our experiments suggest the following reaction

$$ZrC + 2H_2O = ZrO_2 + CH_4 \quad (1)$$

These experimental results confirm that the reaction between ZrC and water under high-temperature and high-pressure conditions produced zirconia.

DOI: 10.1021/acs.jpcc.9b00715
J. Phys. Chem. C 2019, 123, 10051−10056

IV. CONCLUSIONS

In summary, in situ high-pressure XRD studies on ZrC have been performed using DACs with pressure up to ∼154 GPa at room temperature. Our results show that ZrC remains stable rather than undergoing structural phase transition from B1 to B2 as predicted by theoretical calculations. Furthermore, utilizing a double-side laser-heating technology coupled with DACs, the stability of the B1 phase ZrC under HPHT conditions has been explored. Although B1 ZrC shows no polymorphic phase transition at pressures up to 40 GPa and temperatures up to 2000 K, ZrC is incredibly susceptible to even trace amount of water and will react with water to form zirconia along with CH_4 under HPHT conditions. These results clarify the structural and chemical stability of the B1 phase ZrC at extreme conditions, which would guide the application of ZrC and provide new experimental constraint for theoretical calculations. If ZrC is used as a structural component under extreme conditions, water should be carefully removed from the environment to avoid serious corrosion of ZrC. On the other hand, it also indicates that ZrC is likely to be a good desiccant in extreme HPHT environments. Since many of the TMCs typically behave similarly, the phenomena observed in ZrC are expected to be general in other TMCs as well.

■ ASSOCIATED CONTENT

Supporting Information

The Supporting Information is available free of charge on the ACS Publications website at DOI: 10.1021/acs.jpcc.9b00715.

Rietveld refinement result of ZrC at 5 GPa and room temperature (quenched from ∼2000 K) after laser heating; representative SEM image and a typical EDS spectrum of the initial B1 phase ZrC powder (PDF)

■ AUTHOR INFORMATION

Corresponding Authors

*E-mail: zengzd@hpstar.ac.cn (Z.Z.).
*E-mail: pengfang@scu.edu.cn (F.P.).

ORCID

Lijie Tan: 0000-0001-9396-7613

Notes

The authors declare no competing financial interest.

■ ACKNOWLEDGMENTS

This research was supported by the National Thousand Youth Talents Program in China, the National Natural Science Foundation of China (Nos. 51871054 and U1530402), and the Fundamental Research Funds for the Central Universities of China. The in situ high-pressure and high-temperature XRD experiments were mainly carried out at the beamline 12.2.2, Advanced Light Source (ALS) and beamline 13 ID-D (GSECARS), Advanced Photon Source (APS). ALS was supported by the Director, Office of Science, DOE-BES under Contract No. DE-AC02-05CH11231. GSECARS was supported by the National Science Foundation-Earth Sciences (EAR-1634415) and the Department of Energy (DOE), GeoSciences (DE-FG02-94ER14466). Use of the APS was supported by DOE, Office of Basic Energy Sciences (BES), under Contract DE-AC02-06CH11357.

■ REFERENCES

(1) Toth, L. *Transition Metal Carbides and Nitrides*; Academic Press: New York and London, 1971.
(2) Oyama, S. T. *The Chemistry of Transition Metal Carbides and Nitrides*, 1st ed.; Springer: Netherlands, 1996.
(3) Weber, W. Lattice Dynamics of Transition-Metal Carbides. *Phys. Rev. B* **1973**, *8*, 5082−5092.
(4) Alward, J. F.; Fong, C. Y.; El-Batanouny, M.; Wooten, F. Band structures and optical properties of two transition-metal carbides—TiC and ZrC. *Phys. Rev. B* **1975**, *12*, 1105−1117.
(5) Williams, W. S. Transition-metal carbides. *Prog. Solid State Chem.* **1971**, *6*, 57−118.
(6) Williams, W. S. Physics of transition metal carbides. *Mater. Sci. Eng., A* **1988**, *105−106*, 1−10.
(7) Gogotsi, Y. Transition metal carbides go 2D. *Nat. Mater.* **2015**, *14*, 1079.
(8) Xu, C.; Wang, L.; Liu, Z.; Chen, L.; Guo, J.; Kang, N.; Ma, X.-L.; Cheng, H.-M.; Ren, W. Large-area high-quality 2D ultrathin Mo_2C superconducting crystals. *Nat. Mater.* **2015**, *14*, 1135.
(9) Huang, K.; Li, Z.; Lin, J.; Han, G.; Huang, P. Two-dimensional transition metal carbides and nitrides (MXenes) for biomedical applications. *Chem. Soc. Rev.* **2018**, *47*, 5109−5124.
(10) Li, H.; Zhang, L.; Zeng, Q.; Ren, H.; Guan, K.; Liu, Q.; Cheng, L. First-principles study of the structural, vibrational, phonon and thermodynamic properties of transition metal carbides TMC (TM = Ti, Zr and Hf). *Solid State Commun.* **2011**, *151*, 61−66.
(11) Champion, A. R.; Drickamer, H. G. The effect of high pressure on the compressibility of four cubic carbides. *J. Phys. Chem. Solids* **1965**, *26*, 1973−1975.
(12) Zhong, Y.; Xia, X.; Shi, F.; Zhan, J.; Tu, J.; Fan, H. J. Transition Metal Carbides and Nitrides in Energy Storage and Conversion. *Adv. Sci.* **2016**, *3*, No. 1500286.
(13) Kim, J.; Suh, Y. J. Temperature- and pressure-dependent elastic properties, thermal expansion ratios, and minimum thermal conductivities of ZrC, ZrN, and $Zr(C_{0.5}N_{0.5})$. *Ceram. Int.* **2017**, *43*, 12968−12974.
(14) Zaima, S.; Adachi, H.; Shibata, Y. Promising cathode materials for high brightness electron beams. *J. Vac. Sci. Technol., B: Microelectron. Process. Phenom.* **1984**, *2*, 73−78.
(15) Chen, C.-S.; Liu, C.-P.; Tsao, C. Y. A. Influence of growth temperature on microstructure and mechanical properties of nanocrystalline zirconium carbide films. *Thin Solid Films* **2005**, *479*, 130−136.
(16) Kieffer, R.; Benesovsky, F.; Hartstoffe, W. *Springer-Verlag Wien*, 1963; Vol. *10*, pp 7151−6.
(17) Sani, E.; Mercatelli, L.; Francini, F.; Sans, J. L.; Sciti, D. Ultra-refractory ceramics for high-temperature solar absorbers. *Scripta Mater.* **2011**, *65*, 775−778.
(18) Kim, J.; Kang, S. First principles investigation of temperature and pressure dependent elastic properties of ZrC and ZrN using Debye−Gruneisen theory. *J. Alloys Compd.* **2012**, *540*, 94−99.
(19) Huang, Q.; Yu, D.; Xu, B.; Hu, W.; Ma, Y.; Wang, Y.; Zhao, Z.; Wen, B.; He, J.; Liu, Z.; et al. Nanotwinned diamond with unprecedented hardness and stability. *Nature* **2014**, *510*, 250.
(20) Zeng, Z.; Yang, L.; Zeng, Q.; Lou, H.; Sheng, H.; Wen, J.; Miller, D. J.; Meng, Y.; Yang, W.; Mao, W. L.; et al. Synthesis of quenchable amorphous diamond. *Nat. Commun.* **2017**, *8*, No. 322.
(21) Tian, Y.; Xu, B.; Yu, D.; Ma, Y.; Wang, Y.; Jiang, Y.; Hu, W.; Tang, C.; Gao, Y.; Luo, K.; et al. Ultrahard nanotwinned cubic boron nitride. *Nature* **2013**, *493*, 385.
(22) Wang, P.; Kumar, R.; Sankaran, E. M.; Qi, X.; Zhang, X.; Popov, D.; Cornelius, A. L.; Li, B.; Zhao, Y.; Wang, L. Vanadium Diboride (VB_2) Synthesized at High Pressure: Elastic, Mechanical, Electronic, and Magnetic Properties and Thermal Stability. *Inorg. Chem.* **2018**, *57*, 1096−1105.
(23) Wang, S.; Yu, X.; Zhang, J.; Zhang, Y.; Wang, L.; Leinenweber, K.; Xu, H.; Popov, D.; Park, C.; Yang, W.; et al. Crystal structures, elastic properties, and hardness of high-pressure synthesized CrB_2 and CrB_4. *J. Superhard Mater.* **2014**, *36*, 279−287.

DOI: 10.1021/acs.jpcc.9b00715
J. Phys. Chem. C 2019, 123, 10051−10056

(24) Wang, P.; Wang, Y.; Wang, L.; Zhang, X.; Yu, X.; Zhu, J.; Wang, S.; Qin, J.; Leinenweber, K.; Chen, H.; et al. Elastic, magnetic and electronic properties of iridium phosphide Ir_2P. *Sci. Rep.* **2016**, *6*, No. 21787.
(25) Bhardwaj, P.; Singh, S. Structural phase stability and elastic properties of refractory carbides. *Int. J. Refract. Met. Hard Mater.* **2012**, *35*, 115−121.
(26) Abavare, E. K. K.; Dodoo, S. N. A.; Uchida, K.; Nkurumah-Buandoh, G. K.; Yaya, A.; Oshiyama, A. Indirect phase transition of TiC, ZrC, and HfC crystal structures. *Phys. Status Solidi B* **2016**, *253*, 1177−1185.
(27) Singh, A.; Aynyas, M.; Sanyal, S. P. High pressure behavior and structural properties of transition metal carbides. *Phase Transitions* **2009**, *82*, 576−586.
(28) Rathod, N.; Gupta, S. K.; Jha, P. K. Dynamical stability and phase transition of ZrC under pressure. *Phase Transitions* **2012**, *85*, 1060−1069.
(29) Hao, A.; Zhou, T.; Zhu, Y.; Zhang, X.; Liu, R. First-principles investigations on electronic, elastic and thermodynamic properties of ZrC and ZrN under high pressure. *Mater. Chem. Phys.* **2011**, *129*, 99−104.
(30) Lv, Z.; Hu, H.; Wu, C.; Cui, S.; Zhang, G.; Feng, W. First-principles study of structural stability, electronic and elastic properties of ZrC compounds. *Phys. B* **2011**, *406*, 2750−2754.
(31) Chauhan, M.; Gupta, D. C. Electronic, mechanical, phase transition and thermo-physical properties of TiC, ZrC and HfC: High pressure computational study. *Diamond Relat. Mater.* **2013**, *40*, 96−106.
(32) Mao, H. K.; Xu, J.; Bell, P. M. Calibration of the ruby pressure gauge to 800 kbar under quasi-hydrostatic conditions. *J. Geophys. Res.: Solid Earth* **1986**, *91*, 4673−4676.
(33) Fei, Y.; Ricolleau, A.; Frank, M.; Mibe, K.; Shen, G.; Prakapenka, V. Toward an internally consistent pressure scale. *Proc. Natl. Acad. Sci. U.S.A.* **2007**, *104*, 9182.
(34) Caldwell, W. A.; Kunz, M.; Celestre, R. S.; Domning, E. E.; Walter, M. J.; Walker, D.; Glossinger, J.; MacDowell, A. A.; Padmore, H. A.; Jeanloz, R.; et al. Laser-heated diamond anvil cell at the advanced light source beamline 12.2.2. *Nucl. Instrum. Methods Phys. Res., Sect. A* **2007**, *582*, 221−225.
(35) Kunz, M.; MacDowell, A. A.; Caldwell, W. A.; Cambie, D.; Celestre, R. S.; Domning, E. E.; Duarte, R. M.; Gleason, A. E.; Glossinger, J. M.; Kelez, N.; et al. A beamline for high-pressure studies at the Advanced Light Source with a superconducting bending magnet as the source. *J. Synchrotron Radiat.* **2005**, *12*, 650−658.
(36) Prescher, C.; Prakapenka, V. B. DIOPTAS: a program for reduction of two-dimensional X-ray diffraction data and data exploration. *High Pressure Res.* **2015**, *35*, 223−230.
(37) Birch, F. Finite strain isotherm and velocities for single-crystal and polycrystalline NaCl at high pressures and 300 °K. *J. Geophys. Res.: Solid Earth* **1978**, *83*, 1257−1268.
(38) Brown, H. L.; Kempter, C. P. Elastic properties of zirconium carbide. *Phys. Status Solidi B* **1966**, *18*, K21−K23.
(39) Méçabih, S.; Amrane, N.; Nabi, Z.; Abbar, B.; Aourag, H. Description of structural and electronic properties of TiC and ZrC by generalized gradient approximation. *Phys. A* **2000**, *285*, 392−396.
(40) Lu, X.-G.; Selleby, M.; Sundman, B. Calculations of thermophysical properties of cubic carbides and nitrides using the Debye−Grüneisen model. *Acta Mater.* **2007**, *55*, 1215−1226.
(41) Singh, A. K. The lattice strains in a specimen (cubic system) compressed nonhydrostatically in an opposed anvil device. *J. Appl. Phys.* **1993**, *73*, 4278−4286.
(42) He, D.; Shieh, S. R.; Duffy, T. S. Strength and equation of state of boron suboxide from radial x-ray diffraction in a diamond cell under nonhydrostatic compression. *Phys. Rev. B* **2004**, *70*, No. 184121.
(43) Nino, A.; Tanaka, A.; Sugiyama, S.; Taimatsu, H. Indentation Size Effect for the Hardness of Refractory Carbides. *Mater. Trans.* **2010**, *51*, 1621−1626.
(44) Ohtaka, O.; Fukui, H.; Kunisada, T.; Fujisawa, T.; Funakoshi, K.; Utsumi, W.; Irifune, T.; Kuroda, K.; Kikegawa, T. Phase relations and equations of state of ZrO_2 under high temperature and high pressure. *Phys. Rev. B* **2001**, *63*, No. 174108.
(45) Desgreniers, S.; Lagarec, K. High-density ZrO_2 and HfO_2 Crystalline structures and equations of state. *Phys. Rev. B* **1999**, *59*, 8467−8472.
(46) Osei-Agyemang, E.; Paul, J. F.; Lucas, R.; Foucaud, S.; Cristol, S. Periodic DFT and Atomistic Thermodynamic Modeling of Reactivity of H2, O2, and H2O Molecules on Bare and Oxygen Modified ZrC (100) Surface. *J. Phys. Chem. C* **2014**, *118*, 12952−12961.
(47) Osei-Agyemang, E.; Paul, J.-F.; Lucas, R.; Foucaud, S.; Cristol, S. Stability, equilibrium morphology and hydration of ZrC(111) and (110) surfaces with H2O: a combined periodic DFT and atomistic thermodynamic study. *Phys. Chem. Chem. Phys.* **2015**, *17*, 21401−21413.
(48) Wei, B.; Wang, D.; Wang, Y.; Zhang, H.; Peng, S.; Xu, C.; Song, G.; Zhou, Y. Corrosion kinetics and mechanisms of ZrC_{1-x} ceramics in high temperature water vapor. *RSC Adv.* **2018**, *8*, 18163−18174.
(49) Keramidas, V. G.; White, W. B. Raman Scattering Study of the Crystallization and Phase Transformations of ZrO2. *J. Am. Ceram. Soc.* **1974**, *57*, 22−24.
(50) Wu, Y. H.; Sasaki, S.; Shimizu, H. High-pressure Raman study of dense methane: CH_4 and CD_4. *J. Raman Spectrosc.* **1995**, *26*, 963−967.

DOI: 10.1021/acs.jpcc.9b00715
J. Phys. Chem. C 2019, 123, 10051−10056